ATLAS NOTE

July 3, 2008

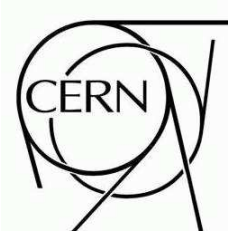

Looking for signatures of the Left-Right Twin Higgs model with the ATLAS detector at the LHC

ATL-PHYS-PUB-2008-004
10 August 2008

S. Ferrag[a], S. Gonzalez de la Hoz[b],L. March[b], E.Ros[b], M. Rijpstra[c], M. Vos[b], M. Vreeswijk[c]

[a] University of Glasgow, UK
[b] IFIC, University of Valencia/CSIC, Spain
[c] NIKHEF, The Netherlands

Abstract

The twin Higgs mechanism has recently been proposed to solve the little hierarchy problem. The phenomenology of this model is presented, and the possibility to observe some of the signatures predicted by this model using the ATLAS detector at the LHC is discussed. The discovery channel for this model, $Z_H \rightarrow e^+e^-$, should be visible in ATLAS with an integrated luminosity of a few fb^{-1} up to a mass of 2 TeV. Several other channels involving heavy gauge boson decay to third generation quarks are investigated. These may provide an unique signature of this model.

1 Introduction

The Higgs mechanism provides a method to explain electroweak symmetry breaking in the Standard Model [1] (SM). The current lower limit on the mass of the Higgs boson is 114 GeV [2] and electroweak precision measurements from LEP set an upper bound of the order 200 GeV [3]. To avoid fine tuning, the leading quadratically divergent radiative corrections to the Higgs mass require the scale of new physics to be of the order of 1 TeV. However, LEP observables, in good agreement with theoretical expectations, disfavour such a low scale for new physics [4]. This problem is sometimes referred to as the *LEP paradox* or the *little hierarchy problem* [5].

Recently, the Twin Higgs mechanism has been proposed as a solution to this paradox [6, 7]. In this model, the Higgs boson emerges as a pseudo-Goldstone boson after the breaking the global symmetry of the model. This global symmetry is a new symmetry, larger than the $SU(2)_L \otimes U(1)_Y$ symmetry[1)] of the electroweak sector of the SM. The symmetry breaking is achieved in such a way that radiative corrections to the Higgs boson are only logarithmically divergent. Thus the model allows for a Higgs boson mass at the electroweak scale of the order of 100 GeV, while the scale for new physics can be much larger, up to 10 TeV, in agreement with LEP data.

Two implementations of the Twin Higgs model have been studied in detail: the mirror Twin Higgs model [7] and the Left-Right symmetric Twin Higgs model [8]. The results presented here refer to this second implementation (LRTH in the following). In the LRTH model, the global symmetry is $U(4) \otimes U(4)$, with a gauged subgroup $SU(2)_L \otimes SU(2)_R \otimes U(1)_Y$. After the Higgs bosons acquire vacuum expectation values, the global symmetry breaks down to $U(3) \otimes U(3)$ and the gauge symmetry $SU(2)_L \otimes SU(2)_R \otimes U(1)_Y$ breaks down to the SM symmetry $SU(2)_L \otimes U(1)_Y$.

In this note several signatures at the LHC of the LRTH are discussed in some detail. In section 2 and 3 the particle spectrum of the model and some relevant aspects of the LHC phenomenology of the model are discussed. In the subsequent sections the discovery reach is studied for three different final states. In section 4 the "golden" discovery channel $Z_H \rightarrow e^+e^-$ is briefly discussed. In sections 5 and 6 the results are presented of a study into the possibility to detect the decay of the heavy gauge boson W_H of the LRTH model into top and bottom quarks. In section 8 the most important findings are summarized. In two appendices the performance of the ATLAS b-tagging algorithms for multi-b-jet final states and very high p_T jets is discussed.

2 Particle spectrum of the LRTH model

The LRTH model contains seven initially massless gauge bosons:

$$Z_R, W_R^{\pm}, Z_L, W_L^{\pm}, B \tag{1}$$

where the indices R, L refer to right-handed and left-handed particles. After the symmetry breaking, all these gauge bosons acquire mass. The observed neutral physical states in this model - the Z and the massless photon of the Standard Model and a heavy neutral gauge boson labelled Z_H - are combinations of the Z_R, Z_L and B. Mixing is not allowed for $W_R^{\pm}$ and $W_L^{\pm}$. The left-handed $W_L^{\pm}$ is identified with the Standard Model charged gauge boson $W^{\pm}$, while the heavy charged gauge boson $W_H^{\pm}$ is purely right-handed. The heavy gauge bosons Z_H and $W_H^{\pm}$ typically have masses of the order of 1 TeV.

The symmetry breaking of the LRTH model can be implemented in its minimal version with just two Higgs doublets $H = (H_L, H_R)$ and $\hat{H} = (\hat{H}_L, \hat{H}_R)$, that transform as $(\underline{2}, \underline{1}, \underline{1})$ and $(\underline{1}, \underline{2}, \underline{1})$*multiplets*[2)] under the gauge group $SU(2)_R \otimes SU(2)_L \otimes U(1)_Y$. In this minimal version, five scalars emerge as physical states after the symmetry breaking. These scalars are labelled:

$$h, h_1^{\pm}, h_2^0, \phi^{\pm}, \phi^0 \tag{2}$$

Out of these five scalars, three are neutral (h, h_2^0 and ϕ^0) and two are charged ($h_1^{\pm}$ and $\phi^{\pm}$). The particle h can be identified with the SM Higgs boson, whereas h_2^0 is a potential dark matter candidate.

The quadratic loop cancellation of radiative corrections to the SM Higgs mass requires in addition the introduction of an additional top singlet. A term $M\bar{q}_L q_R$ allows mixing of the gauge eigenstates to form the physical states, the Standard Model top quark t and its heavy counterpart T. Experimental constraints allow small, but non-zero values for the mixing parameter. This procedure is similar to that in the littlest Higgs model [9] (LH in the following).

[1)] The following notation is used: Y is the weak hypercharge and satisfies $Y = T_{3R} + \frac{B-L}{2}$

[2)] The notation $\underline{2}$ stands for an $SU(2)$ doublet and $\underline{1}$ for a singlet.

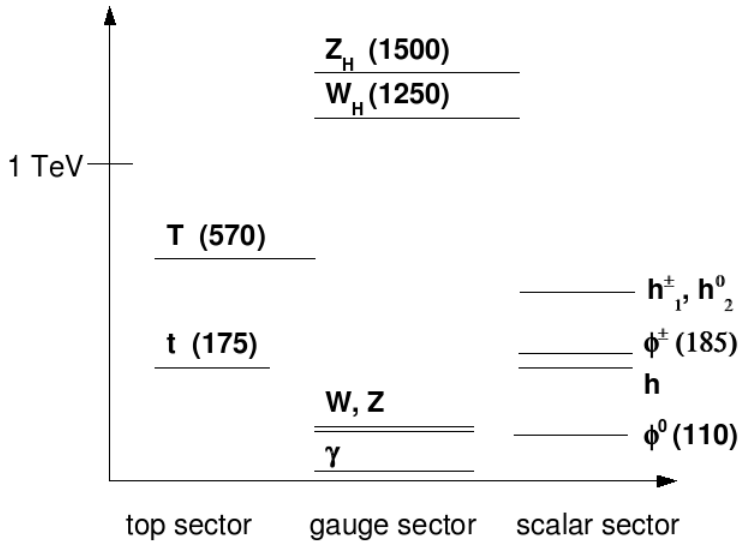

Figure 1: Particle spectrum of the LRTH model, corresponding to the following choice for the model parameters: $f = 555$ GeV, $M = 150$ GeV, $\Lambda = 4\pi f$, $\mu_r = 50$ GeV and $\hat{\mu} = f/2$.

The typical spectrum of particles in the LRTH model is shown in Fig. 1.

The exact shape of the spectrum depends on a small number of model parameters. In the following, the values used are those proposed in [10]. Several benchmark points are used that correspond to values of the Higgs vacuum expectation value f in the range from 500 GeV to 1.5 TeV. This parameter determines the mass of the heavy top quark. The top quark Yukawa coupling is fixed by the light top mass. For each value of f the second Higgs VEV $\hat{f}$, that governs the masses of the heavy gauge bosons, is obtained by minimizing the Higgs potential. For all points $\hat{f} >> f$ and the gauge boson masses are larger than the heavy top mass. A cut-off scale Λ is chosen to be $\Lambda = 4\pi f$. The phenomenology of the model does not depend in a critical way on this choice.

The phenomenology of the LRTH model may be influenced quite strongly by the choice for the remaining free parameters. The parameter M that determines the amount of mixing between the light and heavy top quarks is set to 150 GeV in this study. The collider phenomenology in case $M \to 0$ is discussed in some detail in [10]. In this case the couplings involving heavy gauge bosons and light top quarks (or vice-versa) vanish and some aspects of the phenomenology are affected quite drastically. The Higgs mass parameters, μ_r and $\hat{\mu}$ allow for variations of for the masses of the Higgs bosons in both doublets. The choise of $\hat{\mu} = \hat{f}/2$ that governs the mass of $h_1^{\pm}$ and h_2^0 is largely irrelevant for the studies reported here. A non-zero μ_r is required to avoid a massless ϕ^0 that is experimentally excluded. The chosen value of $\mu_r = 50$ GeV results in relatively light ϕ^0 and $\phi^{\pm}$. The phenomenology is not altered substantially as long as the masses of ϕ^0 and $\phi^{\pm}$ remain smaller than that of the heavy top quarks.

3 Phenomenology of the LRTH model

The phenomenology of the LRTH model is described in detail in Ref. [10, 11] and in this note we follow closely all computations of cross-sections and branching ratios provided in this paper. The most important results cross-sections, masses, widths and branching fractions are listed in table 1 for several benchmark points used in this analysis. For Z_H the cross-sections given in the table were calculated neglecting the interference with the neutral SM gauge bosons Z and γ. For more information, the reader is referred to Ref. [10, 11]

As in any Left-Right symmetric model, the masses of the heavy gauge bosons W_H and Z_H are related through the Weinberg angle:

$$\frac{m(Z_H)}{m(W_H)} = \frac{\cos\theta_w}{\sqrt{1-2\sin^2\theta_w}} \sim 1.20 \tag{3}$$

where we have used a value of 0.23 for $\sin^2\theta_w$.

Table 1: The parameters used in this paper for the most important particles in the LRTH model.

$m(W_H)$ (GeV)	1000	1250	1500	2000	3000
$\Gamma(W_H)$ (GeV)	23.4	29.6	35.6	48.1	72.8
$\sigma(W_H)$ (pb)	27.2	13.2	6.55	1.57	0.18
$m(T)$ (GeV)	487	568	652	812	1144
$m(\phi^{\pm})$ (GeV)	160	184	209	260	363
$m(\phi^0)$ (GeV)	107	109	112	116	119
BR $(W_H \to Tb)$	20.6 %	22.7 %	24.0 %	25.5 %	26.8 %
BR $(W_H \to \phi^{\pm}\phi^0)$	2.7 %	2.7 %	2.7 %	2.8 %	2.8 %
BR $(W_H \to tb)$	4.2 %	2.9 %	2.4 %	1.3 %	0.6 %
$m(Z_H)$ (GeV)	1196	1495	1794	2407	3587
$\Gamma(Z_H)$ (GeV)	24.8	31.2	37.8	51.1	76.5
$\sigma(Z_H)$ (pb)	6.0	2.3	1.0	0.22	0.02
BR $(Z_H \to e^+e^-)$	2.42 %	2.40 %	2.39 %	2.37 %	2.36 %
BR $(Z_H \to Zh)$	0.44 %	0.43 %	0.43 %	0.43 %	0.43 %

As discussed in [10], the most favourable processes to observe particles predicted by the LRTH model at the LHC are Z_H and W_H production.

For the heavy neutral gauge boson Z_H the following decays are predicted:

$Z_H \to q\bar{q}$	BR = 59 % (q = u,d,s,c)
$Z_H \to b\bar{b}$	BR = 19 %
$Z_H \to tT$	BR $\sim$ 4.4 %
$Z_H \to e^+e^-$	BR = 2.5 %
$Z_H \to t\bar{t}$	BR = 2.5 %
$Z_H \to T\bar{T}$	BR = 2.2 %
$Z_H \to Zh$	BR = 0.4 %

The values for the branching ratios are given assuming a heavy gauge boson mass $m(Z_H) = 1.5$ TeV. The branching ratios $Z_H \to e^+e^-$ and $Z_H \to Zh$ are rather independent of mass and model parameters.

The decay $Z_H \to e^+e^-$ is the *golden channel*. Unlike other decays, this decay is present independently of model parameters. However, $Z_H \to e^+e^-$ is not a distinctive signature of the LRTH model, since this decay is present in most extensions of the SM with heavy neutral gauge bosons, and in particular in the LH model. The decay $Z_H \to Zh$, where h is the Standard Model Higgs boson, is more discriminating, but has smaller branching ratio, and is furthermore also present in the LH model.

For the heavy charged gauge boson W_H the following decays are predicted:

$W_H \to e\nu_R$	forbidden
$W_H \to q\bar{q}'$	BR = 68 %
$W_H \to Tb$	BR = 22.7 %
$W_H \to tb$	BR = 2.9 %
$W_H \to \phi^{\pm}\phi^0$	BR = 2.7 %

The decay $W_H \to e\nu_R$ is forbidden under the (likely) hypothesis that $m(\nu_R) > m(W_H)$. In most models (including the Little Higgs model), the heavy charged gauge boson is left-handed, and the decay $W_H \to e\nu_L$ can be observed. The absence of this decay could therefore be an important clue to discriminate the LRTH model from most other models.

The decay $W_H \to tb$ is present, as well. Compared to the Littlest Higgs model, this decay mode has a much reduced branching ratio.

Finally, the decay $W_H \to Tb$ (suppressed in the LH model) is present in the LRTH model and is a unique feature of the model. The subsequent decays of T and $\phi^{\pm}$ give rise to a large number of signatures.

Of the many possible W_H decay modes, the following could be detected by the ATLAS experiment:

$W_H \to Tb$	$\to \phi^{\pm} bb \to 4b + l + E_T^{miss}$	BR ~ 3.3 %
	$\to bWb \to 2b + l + E_T^{miss}$	BR ~ 0.4 %
	$\to thb \to 4b + l + E_T^{miss}$	BR ~ 0.4 %
	$\to tZb \to 2b + 3l$	BR ~ 0.01 %
	$\to t\phi^0 b \to 4b + l + E_T^{miss}$	BR ~ 0.1 %
$W_H \to tb$	$\to 2b + l + E_T^{miss}$	BR ~ 0.6 %
$W_H \to \phi^{\pm}\phi^0$	$\to 4b + l + E_T^{miss}$	BR ~ 0.5 %

where results are quoted for a heavy charged gauge boson mass $m(W_H) = 1.25$ TeV. The signatures of the W_H boson in the LRTH model are multi b-jet final states with typically a lepton and missing transverse energy.

In two of the most interesting decay chains, the decay $\phi^{\pm} \to tb$ is involved. The branching ratio for this decay depends strongly on the value of the tT mixing parameter M. For the value chosen here ($M = 150$ GeV) the branching ratio is nearly 100 %. If the mixing is made very small ($M \to 0$) the branching ratio vanishes and channels involving this decay are no longer accessible.

The cascade decays involving $\phi^{\pm} \to tb$ are furthermore limited to the region of parameter space where the charged Higgs boson mass is larger than the sum of top and bottom quark masses $m(\phi^{\pm}) > m(t) + m(b)$. For the parameters chosen here the minimal value of the Higgs vacuum expectation value ($f > 550$) to allow the decay $\phi^{\pm} \to tb$ corresponds to a minimum W_H mass of 1250 GeV.

4 Study of the decay $Z_H \to e^+e^-$

The discovery channel for the LR twin Higgs model is expected to be the leptonic decay of the heavy Z_H gauge boson.

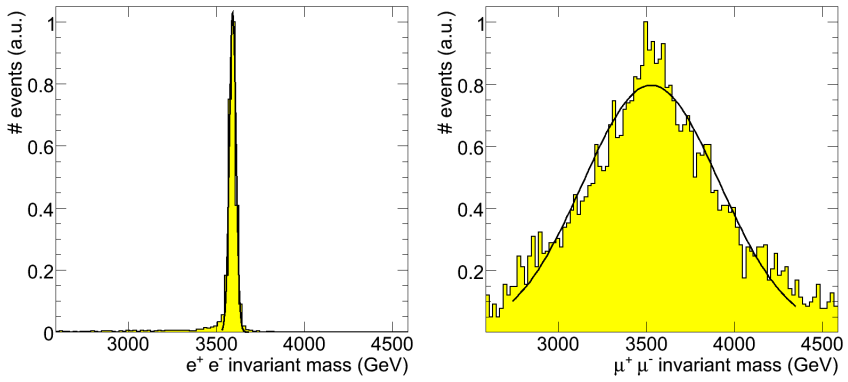

(a) (b)

Figure 2: ATLAS fast simulation: reconstructed invariant mass distribution for a heavy resonance ($m(Z_H) = 3587$ GeV) with a line-shape given by a Dirac δ function. The reconstructed mass distribution is shown for decays into an electron-positron (a) and a muon pair (b).

As the Z_H resonance in the LRTH model is quite narrow, excellent momentum resolution for high p_T leptons is crucial. The invariant mass resolution of the reconstruction of muon pairs and electron-positron pairs is studied using ATLFAST [12]. As expected, the mass reconstruction for very heavy resonances is much more precise in the electron-positron channel, where the p_T resolution is dominated by the electromagnetic calorimeter measurement, than in the di-muon channel. For the benchmark point with the smallest Z_H mass ($m(Z_H) = 1196$ GeV, $\Gamma(Z_H) = 24$ GeV) the mass resolution distribution has a (Gaussian) width of 8 GeV in the electron-positron channel, against 60 GeV in di-muon events.

For very heavy resonances this difference is further enhanced. For the largest Z_H mass considered here ($m(Z_H) = 3587$ GeV, $\Gamma(Z_H) = 75$ GeV) the distributions of Fig 2 are represented fairly well by Gaussians with

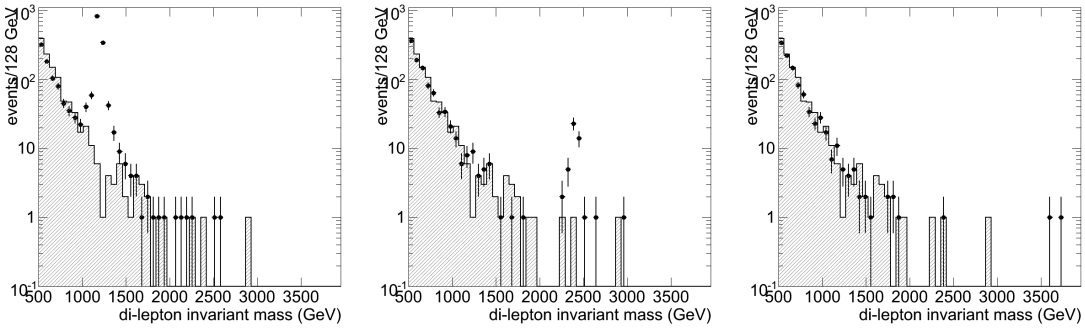

(a) (b) (c)

Figure 3: Pythia generator level: the invariant mass distribution for LRTH $Z/\gamma^*/Z_H$ interference (markers) and the SM Drell-Yan process (histogram with dashed fill). The three figures correspond to Z_H masses of (a) 1196 GeV, (b) 2407 GeV and (c) 3587 GeV.

a width of 19 GeV (electron-positron pairs) or 400 GeV (muon pair). Throughout the mass range studied the experimental electron-positron mass resolution is expected to be well below the natural width of the Z_H boson. Therefore, while the di-muon and di- τ channels are definitely of interest, the following analysis will concentrate on the electron-positron channel.

For each of the benchmark (mass) points, the number of events corresponding to an integrated luminosity of 10 fb $^{-1}$ is generated with Pythia [13]. The Standard Model background is the Drell-Yan process $pp \to Z/\gamma^* \to e^+e^-$, while for the signal the full interference of $pp \to Z/\gamma^*/Z_H \to e^+e^-$ is generated. The signal (markers) and background (dashed line) distributions are shown in Fig. 3 for the benchmark points with $m(Z_H) = 1196$, 2407 and 3587 GeV.

Table 2: Required integrated luminosity to reach a signal significance of 5σ.

$m(Z_H)$ (GeV)	N_{signal} in 10 fb^{-1}	N_{bkg} in 10 fb $^{-1}$	5σ luminosity (fb $^{-1}$)
1196	1123	6	0.04
1495	464	7	0.10
2407	43	1	1.1
3587	2	0	15

For relatively light resonances, as in the leftmost figure in Fig. 3, a clear and narrow peak is observed on top of the exponentially decaying continuum background. For higher masses, as in the case of the central and rightmost figures in Fig. 3, the signal is essentially background-free. Due to the small branching fraction and the rapid decrease of the cross-section for large Z_H mass, the discovery region is limited by the vanishing number of signal events.

The number of signal and background events expected for 10 fb $^{-1}$ in a mass window of 2σ around the generated mass are listed in table 2. Under the resonance peak the signal cross section is at least 40 times higher than the background cross section. Therefore, we may assume that $S >> B$, where S corresponds to the number of signal events and B to the number of background events. For the luminosities where we don't expect any background events, ie. $1 << B$, 5 signal events are assumed to be enough to claim a discovery of the resonance. The required integrated luminosities to discover the Z_H are shown in table 2.

5 Study of the decay $W_H \rightarrow tb$

The $t\bar{b}$ and $\bar{t}b$ decay modes of the heavy gauge boson W_H provide an interesting signature. In reference [14] it is shown that the signal from the equivalent decay mode in the littlest Higgs model can be isolated from the dominant $t\bar{t}$ background for masses in the range 1 - 2 TeV. However, the corresponding cross section times branching ratio in the LRTH model is strongly reduced. For example, for a mass $m(W_H)$ of 1 TeV, it is roughly a factor 8 smaller:

$$\begin{aligned} \sigma(W_H) \times BR(W_H \rightarrow tb) &= 37 \text{ pb} \times 25\% \quad \text{(LH)} \\ \sigma(W_H) \times BR(W_H \rightarrow tb) &= 27 \text{ pb} \times 4.2\% \quad \text{(LRTH)}, \end{aligned} \tag{4}$$

which implies that it is experimentally more challenging to establish its signal. In this section, the discovery potential of the $W_H \rightarrow tb$ channel is investigated for masses $m(W_H)$ of 1, 1.5 and 2 TeV.

The presented analysis is based on three $W_H \rightarrow tb$ samples, containing about 20k events each, with generated masses $m(W_H)$ of 1, 1.5 and 2 TeV respectively. These samples were produced using Pythia and ATLFAST in Atlas Release 12.0.7.1.

Possible background events from $t\bar{t}$, W+jets and single top are considered. An inclusive background sample of 378501 $t\bar{t}$ events is generated using MC@NLO with the requirement that at least one of the top quarks has a transverse momentum of $p_T(top) > 200$ GeV. For background studies at the highest mass value, a second $t\bar{t}$ sample is produced with $p_T(top) > 400$ GeV which contains 285931 events. The official 5200 sample, which contains 404870 leptonic and semileptonic $t\bar{t}$ decays generated with MC@NLO, was used to validate these samples. In addition, the official samples 8240-8251 (containing a total of approximately 110k events) were used to study contributions from $W+$ jets production and the samples 5500-5502 for single top production (containing approximately 24000 events each).

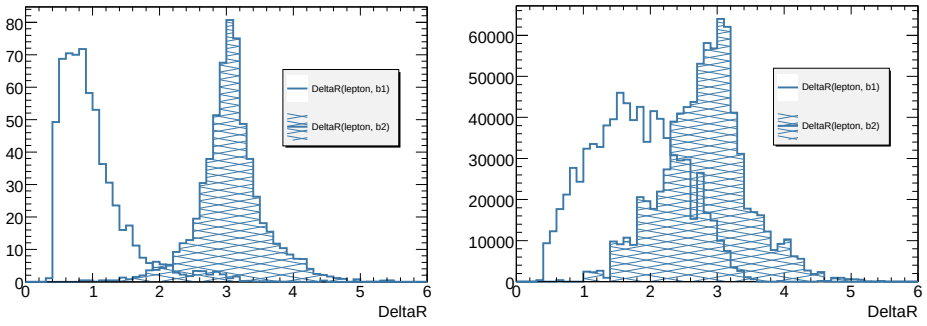

(a) (b)

Figure 4: The distance ΔR of each of the b-jets to the lepton in (a) signal events and (b) in background events.

The experimental signature of $W_H \rightarrow tb$ is determined by the well known decay chain of the top quark ($t \rightarrow Wb$) where the W boson eventually decays either hadronically or leptonically. In this study the focus is on leptonic decays such that the final state contains two b jets, a (charged) lepton and missing transverse energy. The lepton is generally produced with high p_T, providing good trigger possibilities.

The selection procedure in case of $m(W_H) = 1$ TeV is presented in detail in this section, followed by a summary of the selection procedure for the other mass points.

Following [14], the first set of cuts applied to select events with a generated mass of $m(W_H) = 1$ TeV is listed below.

- The presence of exactly 1 lepton, electron or muon, satisfying $p_T > 25$ GeV and $|\eta| < 2.5$ is demanded.
- The missing transverse energy is required to be at least 25 GeV in order to reject QCD events in which a lepton is falsely identified.
- Exactly 2 b-tagged jets with $p_T > 25$ GeV and $|\eta| < 2.5$ are required. To correctly represent the tagging performance for very high p_T jets, a parameterization of results obtained in full simulation is used. More details are given in appendix A. Furthermore, the jets are distinguished according to their distance to the

lepton, $\Delta R(l,b)$ in (η,ϕ) space. The distributions are shown in Figure 4. One of the b-jets is required to be at distance $\Delta R(l,b) < 2$ and is labelled b_1, while the other (b_2) satisfies $\Delta R(l,b) > 2$.

- In figure 5 the p_T distribution of the b-jet furthest from the lepton, $b2$, is shown for signal as well as background events. Events are selected when $p_T > 150$ GeV.

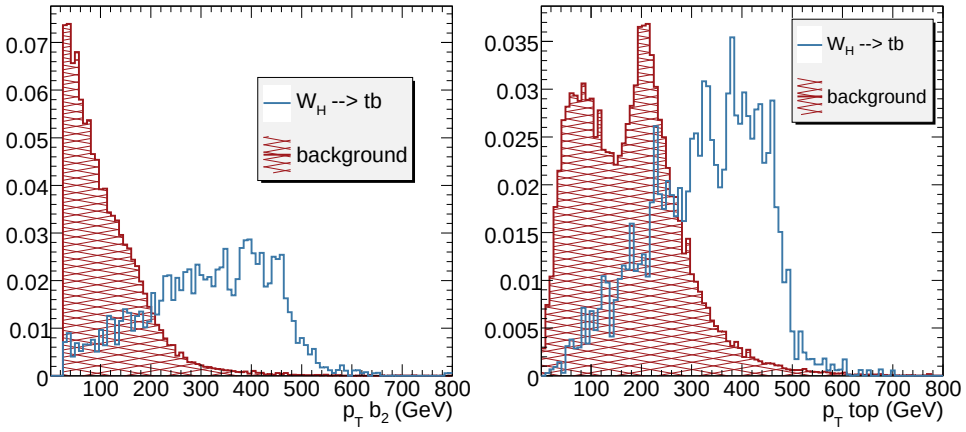

(a) (b)

Figure 5: The normalized distributions of the transverse momentum of the b-jet furthest from the lepton (a), and of the reconstructed top quark candidate (b). The signal events correspond to a W_H mass of 1 TeV

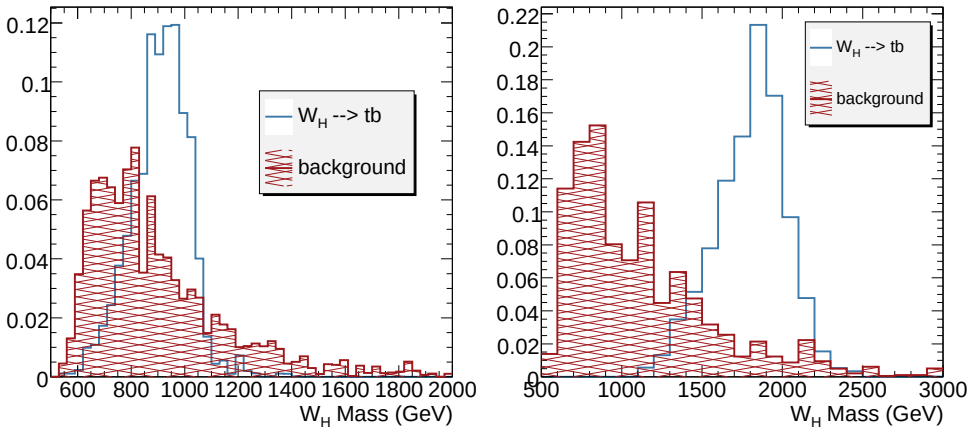

(a) $m(W_H) = 1$ TeV. (b) $m(W_H) = 2$ TeV.

Figure 6: The normalized distributions of the reconstructed W_H mass for signal and background events.

The tagging performance for very high p_T b-jets is modelled on the basis of a full Monte Carlo simulation study [15]. A summary of the results is given in appendix A. The transverse momentum dependent b-tagging efficiencies obtained in this study are implemented for each reconstructed jet, based on the flavour of the quark (b, c or light) to which it is matched at Monte Carlo level. Subsequently, each event obtains a weight corresponding to the probability that it contains exactly two tagged jets. During the reconstruction of the event, the two jets with the highest efficiency are used as b jets.

- The transverse momentum of the top quark is reconstructed by combining b_1, the lepton and $\not{E}_T$. The distributions for signal and background events are shown in Figure 5). Events satisfying $p_T > 250$ GeV pass the selection procedure.

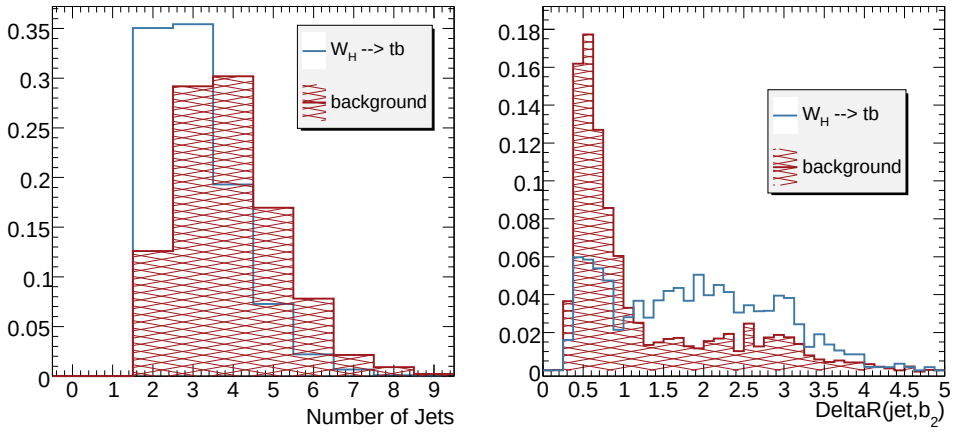

(a) The number of jets in events that passed the basic event selection and satisfy $M(W_H) > 600$ GeV.

(b) The distance of b_2 to the closest additional jet for events that passed the basic event selection and satisfy $M(W_H) > 600$ GeV.

Figure 7: Additional discriminating quantities.

The efficiency of the described event selection is 33 %, tagging efficiencies excluded.

The mass of the W_H is reconstructed by combining the reconstructed momenta of the lepton, b_1, b_2 and the neutrino. The longitudinal momentum p_z^ν of the neutrino is obtained by assuming that the neutrino is produced with the same polar angle as the measured lepton:

$$p_z^\nu = \not{E}_T \frac{p_z^l}{p_T^l} \tag{5}$$

The resulting $m(W_H)$ distributions are shown in Figure 6 for signal and background events respectively. A Gaussian fit to the signal distribution results in a mean value of 929 GeV and a width of 94.9 GeV.

The selection procedure for events with a generated mass $m(W_H)$ of 1.5 TeV is exactly the same as described above, whereas in case of $m(W_H) = 2$ TeV the transverse momenta of b_2 and the reconstructed top are required to be at least 500 GeV. The corresponding selection efficiencies are 21 % and 37 % respectively, tagging efficiencies excluded. The resulting $m(W_H)$ distributions correspond to a mean value of 1384 GeV with a width of 143 GeV in case of a generated mass of 1.5 TeV, and a mean value of 1861 GeV with a width of 177 GeV for a generated mass of 2 TeV.

As opposed to the LH model in [14], the event selection described previously combined with any possible W_H mass window is not sufficient for discovery of this signal in ATLAS due to the smaller branching ratio of the decay channel in the present scenario (Equation 4). In order to reduce the number of remaining background events, of which the majority originate from $t\bar{t}$ production, several additional discriminating quantities are introduced in this section.

Naively, the number of expected jets is 4 in semileptonic $t\bar{t}$ events, while for signal events this number is 2. However, jets can be lost due to overlap with other jets and additional jets can be produced by QCD radiation. Nonetheless, the number of jets in the event, for jets satisfying $p_T > 25$ GeV and $|\eta| < 2.5$, shows different behaviour for signal events compared to background events as can be seen in Figure 7(a).

For semileptonic $t\bar{t}$ events that passed the basic selection criteria, the two light jets from the hadronically decaying W are expected to be produced close to the b_2 jet, due to the boost of the corresponding top quark. This is confirmed by the distribution of the distance $\Delta R(jet, b2)$ of the closest additional jet to b_2 as shown in Figure 7(b).

Based on Figures 7(a) and 7(b), the following set of cuts is applied to suppress the background events:

- Events that contain at most 2 additional jets to b_1 and b_2 are selected.

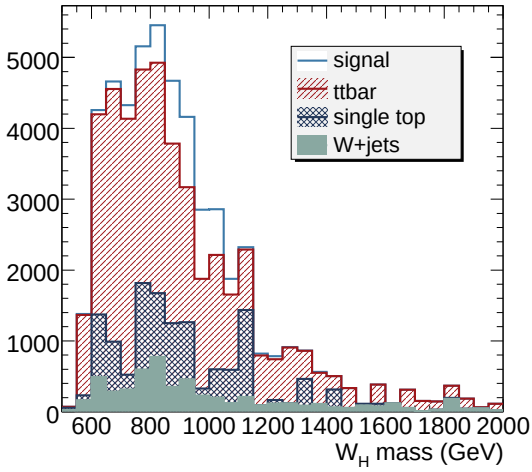

Figure 8: The reconstructed W_H mass for events that passed the basic event selection and the additional cuts. The number of events corresponds to 300 fb^{-1}.

$m(W_H)$ Mass Window	1 TeV [900,1000]	1.5 TeV [1250,1550]	2 TeV [1600,2400]
$t\bar{t}$ Events	9241 $\pm$ 713	2036 $\pm$ 327	667$\pm$ 61
W+jets Events	1809 $\pm$ 552	529 $\pm$ 113	757 $\pm$127
single top Events	3325 $\pm$ 956	806 $\pm$ 412	802 $\pm$ 365
Background Events	14375 $\pm$ 1314	3371 $\pm$ 538	2225$\pm$ 391
Signal Events	3382 $\pm$ 146	441 $\pm$ 19	39 $\pm$ 2
$\frac{S}{\sqrt{B}}$	28	7.6	0.83
$\frac{S}{B}$	0.24	0.13	0.018

Table 3: Summary of the results for an integrated luminosity of 300 fb^{-1}

- In events with one or two additional jets, the distance $\Delta R(jet,b2)$ from the closest jet to b_2 is required to satisfy $\Delta R(jet,b2) > 1$.

After applying the extended selection, the resulting distribution for the reconstructed W_H mass is shown in Fig. 8. The number of events corresponds to a luminosity of 300 fb^{-1}. In the mass window around the central value of the signal, $|M(W_H) - 900|$ <100 GeV, the number of signal events is 3382. The number of background events in this window is 14375. A statistical significance of the W_H signal of 28 is found for a mass of 1 TeV. The same procedure was followed for events with generated masses $m(W_H)$ of 1.5 and 2 TeV and the results are summarized in Table 3.

The $W_H \to tb$ signature of the LRTH model yields a statistical signficance beyond that required for discovery for W_H masses up to 1.5 TeV. However, due to the relatively small S/B ratio and the similarity in shape of signal and background mass distributions the analysis is quite vulnerable to systematic uncertainties in the background level. The selection developed in this note is not able to further improve the robustness of the signal.

If the same selection is applied to the Little Higgs model, where the cross section times branching ratio of the W_H boson is much larger, a significance ($S/\sqrt{B}$) of 230 is obtained, for a S/B-ratio of 1.9.

6 Study of the decay $W_H \to Tb$

The decay of the heavy gauge boson W_H into a heavy top quark T and a b-quark gives rise to distinctive feature of the Left Right Twin Higgs model. In particular, discovery of the cascade decay provides a model test to distinguish

the LRTH model from the LH model.

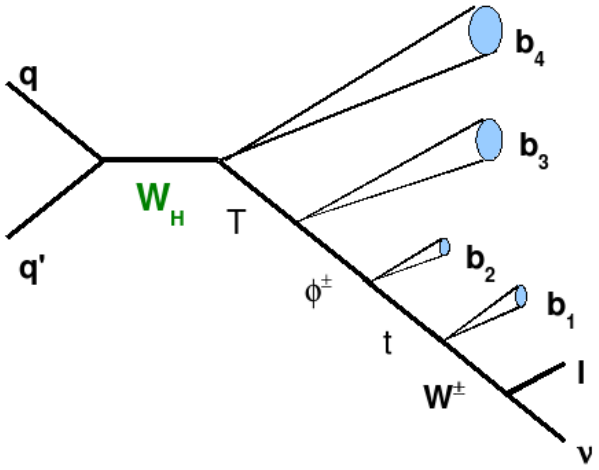

Figure 9: Schematic display of a cascade decay of the W_H boson to a final state with four b-quarks a lepton and a neutrino (missing transverse energy).

Nearly two thirds of W_H bosons decay to a pair of quarks from the first or second family (ud or cs). Isolation of this signal is deemed impossible due to the large QCD background. The next-largest branching fraction - between 20 and 27 % depending on the benchmark point considered - is to a heavy top quark and a b-quark (Tb). In the subsequent T decay, the $T \to \phi^{\pm} b$ channel dominates, with branching fractions ranging from 80 % for lowest mass points, to 95 % for the heaviest W_H boson considered. The charged Higgs boson $\phi^{\pm}$ decays to $\bar{t}b$ or $t\bar{b}$ with close to a 100 % probability, for all benchmark points where this decay is kinematically allowed. For the model parameters considered here, this channel is open for $m(W_H) > 1200$ GeV. The top quark decays to Wb. To facilitate the reconstruction of the decay kinematics and provide a high p_T lepton for the trigger, only W-decays into $l\nu_l$, where l is an electron or a muon, are considered. The complete decay chain then reads: $W_H \to Tb \to \phi^{\pm} bb \to tbbb \to Wbbbb \to l\nu_l bbbb = 4b + l + E_T^{miss}$. The product of all branching fractions is 3.2 %.

Samples of signal events for several different W_H masses and background samples corresponding to $t\bar{t}$ and $W+$ jets have been generated. The whole Monte Carlo production chain is implemented within version 12.0.6 of the ATLAS software framework ATHENA. The signal events are generated with Pythia [13], as well as the reducible *W+jets* background. For the dominant Standard Model $t\bar{t}$ background the MC@NLO [16, 17] generator is used. The detector response is taken into account using the ATLFAST [12] simulation package.

A kinematical reconstruction of the decay chain is performed. The values of the cuts employed in the selection vary with W_H mass. In the following, the selection values for a reconstruction aimed at a 1.25 TeV W_H-bosons are given.

- Events are pre-selected by requiring a minimum lepton transverse momentum of 25 GeV and a minimum missing transverse energy of 25 GeV. The W is reconstructed from the missing transverse energy and the lepton momentum using the collinear approximation (i.e. assuming $p_z^{\nu} = \not{E}_T \frac{p_z^l}{p_T^l}$)
- In the next step, the W candidate is combined with all jets with $25 < p_T(j) < 200$ GeV and the combination that gives the best match with the top mass is selected. If none of the combinations yields a mass $m(t) <$ 250 GeV, the event is discarded.
- A second jet with $25 < p_T < 100$ GeV is added to reconstruct the charged Higgs boson $\phi^{\pm}$. Again, events with a reconstructed $\phi^{\pm}$ mass greater than 250 GeV are discarded.
- A third jet with $p_T(j) > 100$ GeV is required to reconstruct the heavy top quark T. The T-candidate is required to satisfy the following constraints: $m(T) < 700$ GeV and $p_T(T) > 150$ GeV. This latter cut,

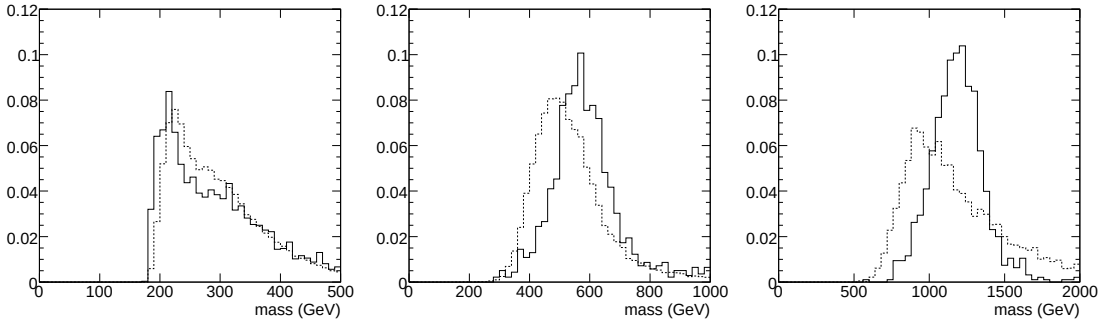

(a) $\phi^{\pm}$ candidate (b) T candidate (c) W_H candidate

Figure 10: ATLAS fast simulation: mass distributions for different steps of the reconstruction of the decay chain for signal events (full line) and the dominant $t\bar{t}$ background (dashed histogram).

that takes advantage of the Jacobean peak in the signal, is particularly useful to reduce the dominant $t\bar{t}$ background.

- Finally, a fourth jet with $p_T(j) > 150$ GeV is used to form the W_H candidate.

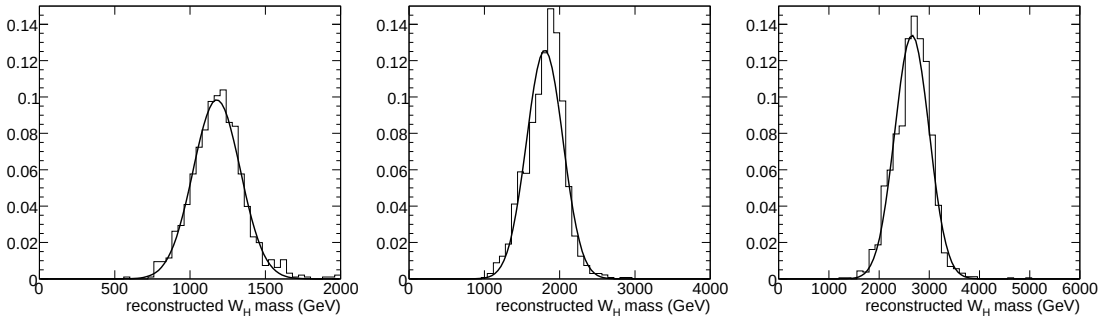

(a) (b) (c)

Figure 11: ATLAS fast simulation: invariant mass distribution of the heavy charged gauge boson after the full kinematical reconstruction. The plots from left to right correspond to generated masses of (a) 1250, (b) 2000 and (c) 3000 GeV.

The reconstructed mass distributions for the different particles involved in the decay chain are shown in Fig. 10. The total efficiency for the kinematical reconstruction is 12 %.

The distribution for the reconstructed W_H mass is shown in Fig. 11. The central value is typically quite a bit lower than the generated mass. The distribution has a width between 160 GeV (for the 1.25 TeV point) and 340 GeV (for the 3 TeV point). In all cases the reconstructed distribution is significantly broader than the natural width of the W_H boson (ranging from 30 to 70 GeV for these mass points).

The mass distribution corresponding to a total integrated luminosity of 30 fb^{-1} is shown in Fig. 12 for three different W_H masses. The data points with error bars represent the observation: i.e. the sum of signal and background contributions. The contribution due to background events is indicated in the filled histogram. Quantitative results - the numbers of signal and background events that are found to survive the kinematical reconstruction - are listed in table 4. While the statistical significance of the contribution of the new physics (expressed as the number of signal events divided by the square root of surviving background events) is relatively large, discovery potential for these final states can hardly be claimed. The number of signal and background events (especially for the smallest mass) is such that even a small uncertainty in the background production cross-section or selection efficiency leads to a strong reduction of the significance. The similarity of signal and background mass distributions,

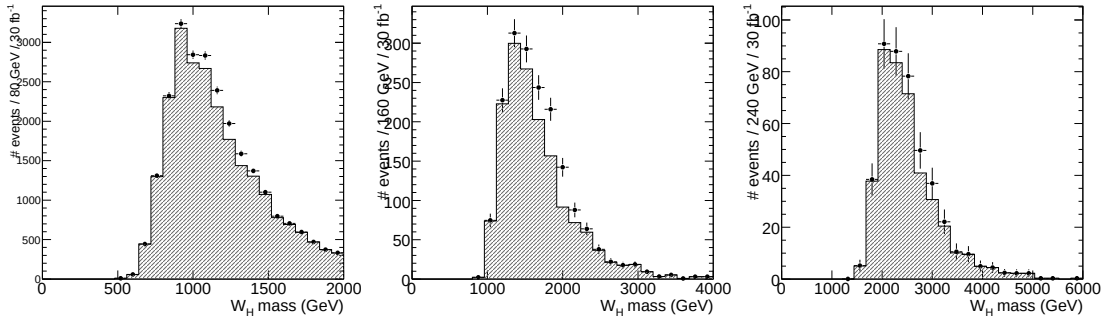

(a) (b) (c)

Figure 12: ATLAS fast simulation: mass distribution of the heavy charged gauge boson candidates after the full kinematical reconstruction and selection procedure. No b-tagging is applied. The contribution of the $t\bar{t}$ and $W + jets$ backgrounds is indicated by the shaded region. The plots from left to right correspond to generated masses (from left to right) of 1250, 2000 and 3000 GeV. These results correspond to an integrated luminosity of $30 fb^{-1}$.

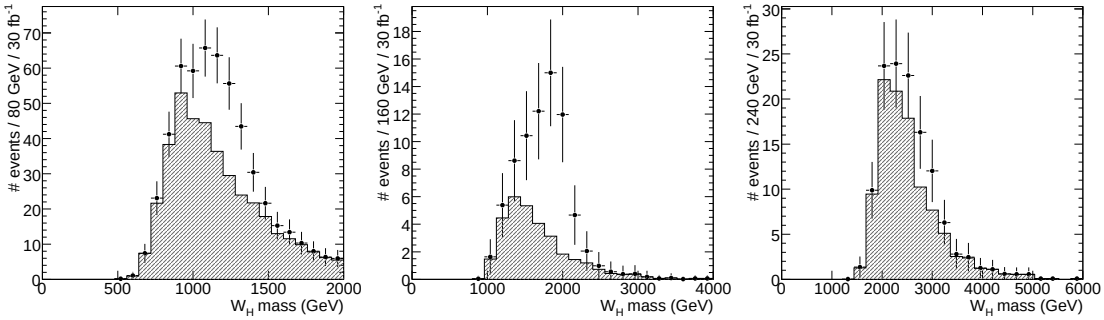

(a) (b) (c)

Figure 13: ATLAS fast simulation: reconstructed mass distribution of W_H candidates (data points) after application of the selection based on the 4 b-jet likelihood. The contribution of the $t\bar{t}$ and $W + jets$ backgrounds is indicated by the shaded region. The plots from left to right correspond to generated masses of (a) 1250, (b) 2000 and (c) 3000 GeV. These results correspond to an integrated luminosity of $30 fb^{-1}$.

a direct result of the procedure used for the kinematical reconstruction of the W_H candidate, effectively prevents a side-band determination of the background level.

The signal signature contains four b-jets, while for the dominant $t\bar{t}$ background two of the jets originate from a b-quark. To further reduce the background, the b-tagging likelihoods of the four jets are combined into one, as described in appendix B. The combined four-jet b-tagging likelihood is found to yield a strong rejection of the background, while retaining a large fraction of the signal events. In the analysis of the 1.25 TeV point, the working point is chosen at 13 % signal efficiency, where a rejection of 60 is obtained for the $t\bar{t}$ background. For larger values of the W_H mass the focus of the b-tagging shifts from large background rejection, to better signal efficiency. In table 4 the number of signal and background events are given after application of the selection based on the four-jet b-tagging likelihood. For all mass points, the $S/\sqrt{B}$ is improved or remains unaltered, but the S/B ratio is greatly improved.

The results in table 4 are not as promising as the preliminary results reported in an earlier study [11]. The main source of difference stems from the use of MC@NLO [16] instead of Pythia [13] for the generation of the Standard Model $t\bar{t}$ background. The much harder p_T spectrum of the top quarks in the former generator leads to a significant increase of the contribution of to the background level after the kinematical reconstruction.

A reconstruction of the cascade decay $W_H \to Tb \to 4b + l + E_T^{miss}$ is therefore one of the most promising analyses in the LRTH model. For the model parameters considered here, this channel provides a mass reach of

Table 4: The number of signal and background events corresponding to an integrated lumonisity of 30 fb^{-1}. For each mass points two columns indicate the number of events after kinematical reconstruction of the W_H decay chain and that after application of a selection based on the four-jet likelihood.

W_H mass (TeV)	1.25		2.0		3.0	
selection	no b-tag	b-tag	no b-tag	b-tag	no b-tag	b-tag
signal	1058	138	217	43	31	22
$t\bar{t}$	23500	392	1560	31	412	103
$W+$ jets	185	-	5	-	3	-
$S/\sqrt{B}$	6.9	7.0	5.5	7.8	1.5	2.2
S/B	0.05	0.4	0.1	1.4	0.08	0.2

greater than 2 TeV with an integrated luminosity of 30 fb $^{-1}$. Detection of this decay provides a valuable model test against other models giving rise to $Z_H \to e^+e^-$, in particular the LH model.

7 Study of the decay $W_H \to \phi^{\pm}\phi^0$

The decay of the heavy gauge boson W_H into a charged and neutral Higgs boson ($W_H \to \phi^{\pm}\phi^0$) has a branching fraction of slightly less than 3 %. In the LRTH model the neutral Higgs boson is light ($\sim$ 110 GeV) and preferentially decays to b-quarks (B.R. $(\phi^0 \to b\bar{b}) \sim 86$ %). The charged Higgs boson $\phi^{\pm}$ decays to tb with a branching fraction of nearly 100 %.

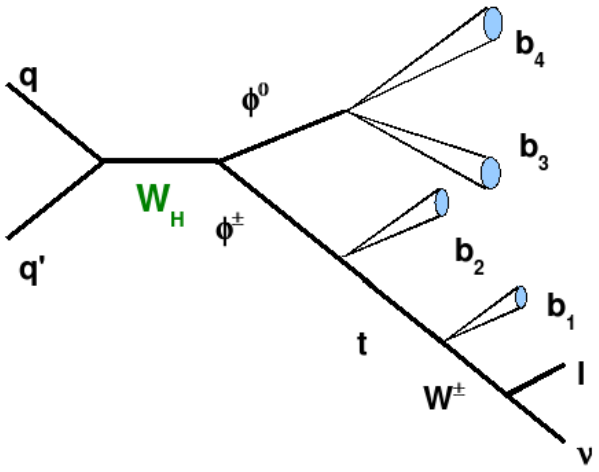

Figure 14: Schematic display of a cascade decay of the W_H boson into charged and neutral Higgs bosons, leading to a final state with four b-quarks a lepton and a neutrino (missing transverse energy).

The schematic diagram of figure 14 indicates how the decay $W_H \to \phi^{\pm}\phi^0$ gives rise to the same $4b+l+E_T^{miss}$ final state as in the previous analysis. The total branching fraction for the cascade decay is however only 0.5 %.

The same backgrounds corresponding to $t\bar{t}$ and $W+$ jets production as in the previous section are considered. The signal process is generated with Pythia [13], while the dominant $t\bar{t}$ background is generated with MC@NLO [16, 17]. The detector response is taken into account using the ATLFAST [12] parametrized simulation package.

A reconstruction of the decay chain along the lines of the previous section is performed. In the following, the cut values for a reconstruction aimed at a 1.25 TeV W_H-bosons are given.

- Events are pre-selected by requiring a minimum lepton transverse momentum of 25 GeV and a minimum missing transverse energy of 25 GeV. The W is reconstructed from the missing transverse energy and the

lepton momentum using the collinear approximation (i.e. assuming $p_z^\nu = \not{E}_T \frac{p_z^l}{p_T^l}$).

- In the next step, the W candidate is combined with all jets with $25 < p_T(j) < 300$ GeV and the combination that gives the best match with the top mass is selected. If none of the combinations yields a mass $m(t) <$ 250 GeV, the event is discarded.
- A second jet with $25 < p_T < 150$ GeV is added to reconstruct the charged Higgs boson $\phi^\pm$. Again, events with a reconstructed $\phi^\pm$ mass greater than 250 GeV are discarded. The transverse momentum of the resulting $\phi^\pm$ is required to be greater than 300 GeV.
- Two further jets with $p_T > 25$ GeV are combined to form the neutral ϕ^0. Events with a reconstructed ϕ^0 mass greater than 150 GeV are discarded. The transverse momentum of the resulting ϕ^0 is required to be greater than 300 GeV.
- Finally, the candidates for the charged and neutral Higgs boson are combined to reconstruct the W_H boson candidate.

For relatively light W_H boson the kinematical reconstruction yields similar results to those of the analysis reported in section 6. The reconstruction efficiency is 8 % for $m(W_H) = 1250$ GeV. As in the previous analysis the mass resolution of ~ 100 GeV is dominated by the reconstruction. Therefore, for relatively light W_H boson, this channel may add to the overall significance of the model, despite the small branching ratio.

It is found, however, that for large W_H masses (of the order of 2-3 TeV) the efficiency of the kinematical reconstruction is degraded. This effect can be understood from the relatively small masses of the Higgs bosons, and particularly for the neutral ϕ^0, with $m(\phi^0) \sim 110$ GeV. The ϕ^0 and $\phi^\pm$ formed in the decay of a 2-3 TeV resonance are strongly boosted and the products of their decays ($\phi^0 \to b\bar{b}$ and $\phi^\pm \to tb$) are emitted at very small angles. The two b-jets from ϕ^0 decay are reconstructed as a single high p_T object and the kinematical reconstruction applied at lower masses is no longer successful. The discovery reach for the cascade decay $W_H \to \phi^\pm\phi^0 \to 4b + l + E_T^{miss}$ with the current reconstruction strategy is therefore limited to small masses ($m(W_H) \sim 1.25$ TeV) of the W_H boson.

A reconstruction of the cascade decay $W_H \to \phi^\pm\phi^0 \to 4b + l + E_T^{miss}$ can provide additional information for model discrimination. For the model parameters considered here, this channel provides a limited mass reach: ATLAS should be able to observe a significant excess of signal events only for masses around 1.25 TeV.

8 Conclusions

The Left Right twin Higgs model offers a solution to the little hierarchy problem. A global LR symmetry leads to the cancellation of quadratically divergent terms due to radiative corrections to the Higgs mass. Heavy gauge bosons Z_H, W_H arise naturally in the model and a heavy partner to the top quark is introduced, giving rise to a rich phenomenology at the LHC.

A set of benchmark (mass) points has been defined for the model parameters and several signatures have been investigated using the ATLAS fast simulation package ATLFAST.

A likely discovery channel is found in the leptonic decay of Z_H. The electron-positron signature is expected to yield a 5σ significance with only 10 fb $^{-1}$ for masses up to 2 TeV.

Signatures from the decay of heavy gauge bosons into third generation quarks have been studied in quite some detail. The reconstruction method for $W_H \to tb$, developed originally for the equivalent signal in the Little(st) Higgs model, has been refined for this analysis. Analysis of an integrated luminosity of 300 fb^{-1} yields a significant signal for masses of the W_H boson of less than 1.5 TeV.

Another signature is the cascade decay $W_H \to Tb \to 4b + l + E_T^{miss}$. A kinematical reconstruction of the decay chain, in combination with a cut on the combined likelihood for the four b-jets, allows the signal to be efficiently isolated from the dominant $t\bar{t}$ and $W+$ jets backgrounds. A statistically significant excess of events is expected to be found in 30 fb $^{-1}$ of data for W_H masses up to 2 TeV.

9 Acknowledgements

The authors would like to thank Shufang Su for her help in determining the parameters of the benchmark points.

A High p_T b-tagging

To take advantage of the large b-jet multiplicity in decays of the W_H boson in the LRTH model, the tagging performance for very high p_T b-jets is essential. The reconstruction of high p_T jets presents a series of specific challenges. In particular, full MC studies have found that the core of dense, collimated jets challenges the pattern recognition performance of the ATLAS inner detector. As a result, the ATLAS flavour tagging performance is found to be significantly degraded for very high p_T jets.

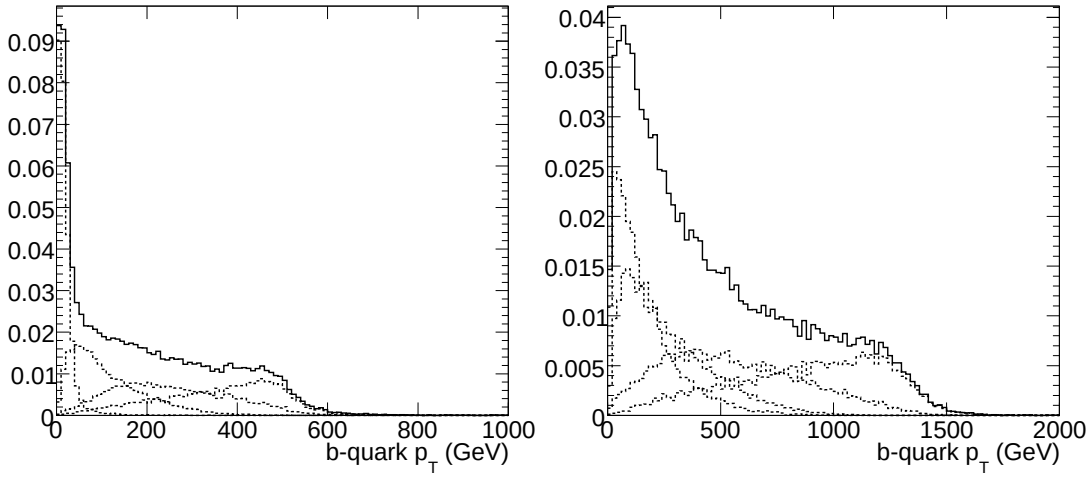

(a) (b)

Figure 15: ATLAS fast simulation: transverse momentum spectrum for the four b-quarks in the cascade decay $W_H \to Tb \to \phi^{\pm} bb \to tbbb \to Wbbbb$. The dashed lines represent the distributions of each of the four b-quarks in the cascade decay, while the continuous line corresponds to the sum of the four distributions. The figures correspond to a W_H mass of 1.25 TeV (a) and 3 TeV (b).

A Monte Carlo study of the high p_T flavour tagging performance is reported in reference [15]. Importantly, in this study the detector response has been simulated using the full detail of the ATLAS detector desciption. Events are reconstructed using release 12.0.6 of the ATLAS software framework ATHENA. Two track reconstruction algorithms have been used and the standard ATLAS flavour tagging algorithms have been retuned to work optimally on high p_T jets. The studies reported in this note rely on parameterizations of these full MC results. In this appendix, specific results are presented for the LRTH signatures that rely on b-tagging.

The transverse momentum distribution of reconstructed b-jets in the analysis of the $W_H \to tb$ channel was shown in figure 5. If the decaying heavy new particle has a mass in the range 1-2 TeV, the b-jets acquire transverse momenta that reach 500 GeV to 1 TeV.

The b-quarks in the cascade decay of heavy W_H bosons are produced in a large range of transverse momenta. Particularly the b-quark stemming from the $W_H \to Tb$ decay and from the $T \to \phi^{\pm} b$ decay attain large momenta. The spectrum for all four b-quarks in the final state is shown in Fig. 15. For a W_H boson with a mass of 1.25 TeV (leftmost figure) the average transverse momentum of the two highest p_T b-quarks exceeds 200 GeV. For larger W_H masses the tail of the transverse momentum distribution extends beyond 1 TeV. Typically, the two very high p_T b-quarks are accompanied by b-quarks with more moderate momenta. Thus, efficient identification of all b-jets in the event, requires a tagging algorithm that yields a good performance throughout a large p_T range.

The b-tagging performance, given in terms of the light jet and c-jet rejection for fixed b-tagging efficiencies of 40 %, 50 % and 60 %, is presented in Fig. 16.

The likelihood distributions returned by the tagger algorithm are parameterized for a number of bins in jet p_T. In the $W_H Tb$ analysis, the parameterized jet likelihoods are combined into an event likelihood, as described in appendix B.

In the analysis of the $W_H \to tb$ channel b-tagging is used to reduce the $W + jets$ background. In this case a fixed cut on the SV1+IP3D likelihood can be used. The evolution of the light jet, c-jet and b-jet efficiency with jet transverse momentum shown in Fig. 16.

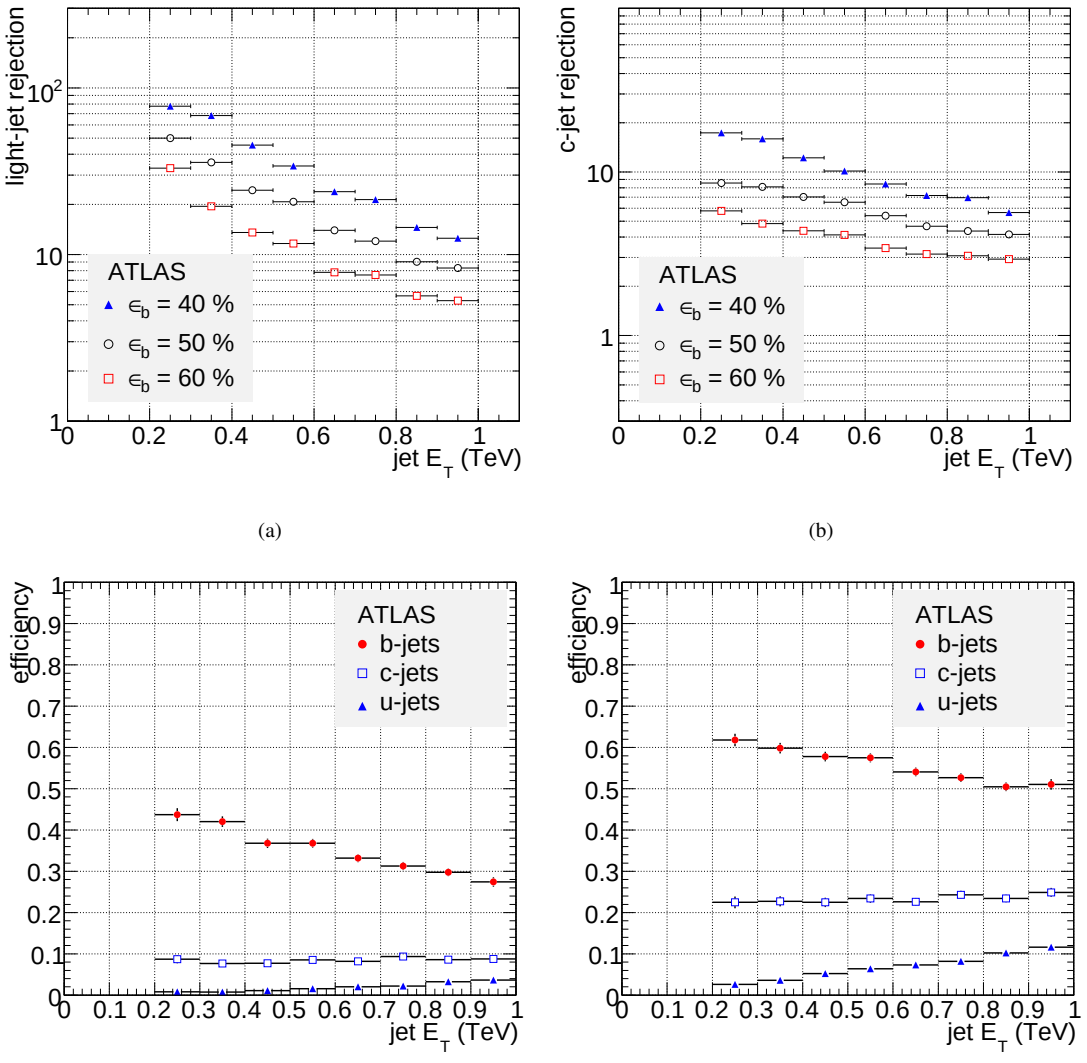

Figure 16: Light jet (a) and c-jet (b) rejection with the combined SV1 + IP3D algorithm versus jet p_T for b-tagging efficiencies of 40 %, 50 % and 60 %. Efficiency for light jets, c-jets and b-jets to satisfy a selection based on the combined SV1 + IP3D likelihood versus jet transverse energy for a fixed likelihood cut 7.9 (c) or 3.5 (d).

B Multi b-jet final states

In section 6 on the cascade decay $W_H \to Tb$ a selection based on b-tagging information is used to isolate the signal with four b-jets from the dominant background after kinematical reconstruction ($t\bar{t}$ production with two b-jets). Requiring at least a certain number of tagged jets yields a sub-optimal performance. Therefore a method to tag multi b-jet final states has been developed, where a four-jet likelihood is constructed by summing the b-tagger log-likelihoods of the four jets with largest tranvserse momentum:

$$w_{event} = \sum_{jets} w_j \tag{6}$$

To be able to apply this method on fast-simulation results, the existing ATLFAST model for b-tagging has been extended to include a parameterization of likelihood distributions from full simulation. Given the large range of jet transverse momenta, it is crucial that the b-tagging performance at high p_T is modelled correctly.

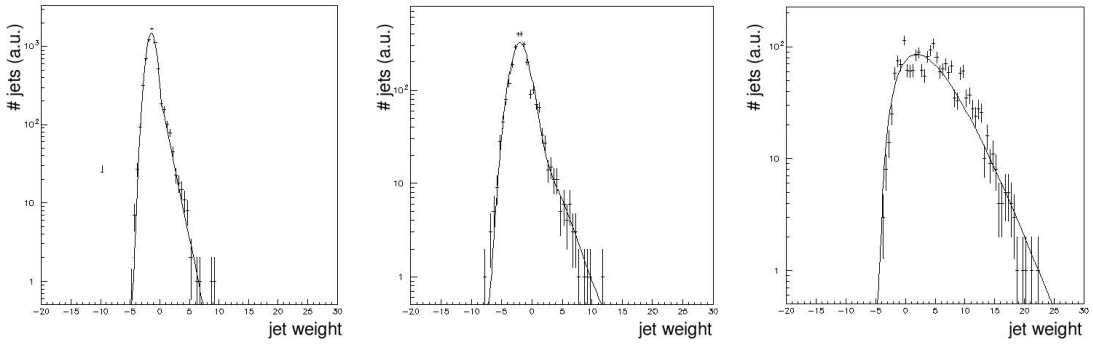

(a) (b) (c)

Figure 17: The jet likelihood distribution from full simulation for light jets (leftmost figure), charm jets (central figure) and b-jets (rightmost figure). These results correspond to the jet p_T interval from 60 to 100 GeV.

In the ATLAS fast simulation package (ATLFAST) the likelihood information has been added by using parameterization of the distribution from full simulation. An example of the distributions for light, charm and b-jets in the p_T range between 60 and 100 GeV is shown in Fig. 17.

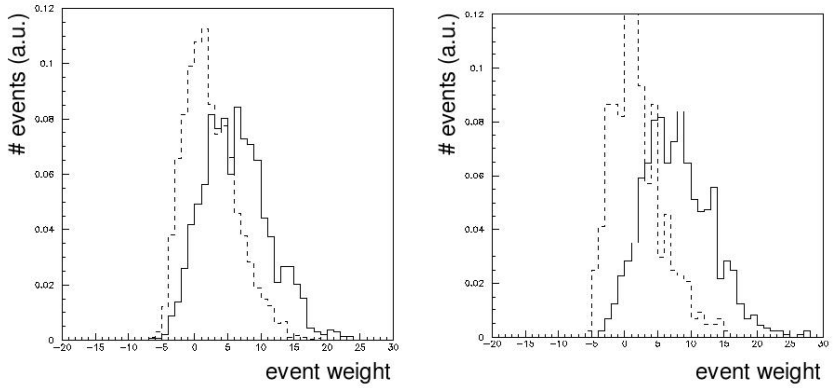

(a) $W_H \to Tb$ (b) $W_H \to \phi^{\pm}\phi^0$

Figure 18: The four-jet likelihood distribution obtained by summing the b-tag (log) likelihoods of the four most energetic jet in the signal (full line) and background events (dashed line).

The four-jet likelihood distributions for signal (full line) and background (dashed line) events are shown in Fig. 18. The leftmost and rightmost figure represent the cascade decay initiated by $W_H(1250) \to Tb$ and $W_H(1250) \to \phi^{\pm}\phi^0$ discussed in sections 6 and 7, respectively.

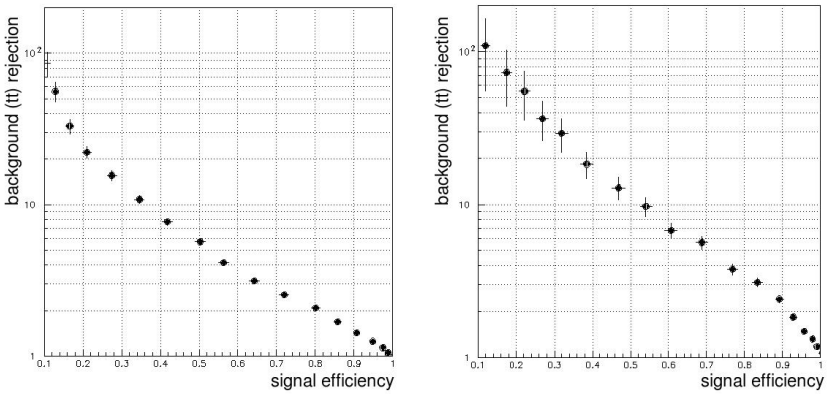

(a) $W_H \to Tb$ (b) $W_H \to \phi^{\pm}\phi^0$

Figure 19: The efficiency vs. rejection curves for the two analyses.

Integration over all bins above a certain cut value yields the rejection vs. efficiency curves in Fig. 19. In the case of the $W_H(1250) \to Tb$ cascade decay (leftmost figure) a background ($t\bar{t}$) rejection of a factor 25 is obtained for a 20 % signal efficiency. In the $W_H(1250) \to \phi^{\pm}\phi^0$ analysis, the working point is set to 40 %, with a factor 20 rejection.

For larger masses, the number of signal and background events is significantly reduced. Therefore, the working point is moved towards larger efficiency and smaller rejection, by a different choice of the four-jet likelihood cut.

References

[1] S. Weinberg, Phys. Rev. Lett. 19 (1967) 1264

[2] The LEP Higgs working group (R. Barate et al.), Search for the standard model Higgs boson at LEP, Phys.Lett.B565 (2003) 61-75

[3] the LEP electroweak working group, Precision electroweak measurements and constraints on the Standard Model, LEPEWWG/2007-01, arXiv:0712.0929

[4] The ALEPH, DELPHI, L3, OPAL, SLD Collaborations, the LEP Electroweak Working Group, the SLD Electroweak and Heavy Flavour Groups, Precision Electroweak Measurements on the Z Resonance, Phys. Rept. 427 (2006)

[5] This problem has been discussed many times. See for example R. Barbieri and A. Strumia, The 'LEP paradox', hep-ph/0007265 and references therein.

[6] R. Barbieri, T. Gregoire and L.J. Hall, Mirror world at the large hadron collider, hep-ph/0509242; Z. Chacko, Y. Nomura, M. Papucci and G. Perez, Natural little hierarchy from a partially goldstone twin Higgs, JHEP 0601 (2006) 126; R. Foot and R.R. Volkas, Natural electroweak symmetry breaking in generalised mirror matter models, Phys.Lett.B645 (2007) 75-81,2007 [hep-ph/0610013]. H.S. Goh, C.A. Krenke, A Little Twin Higgs Model, Phys. Rev. D76 (2007) 115018,2007 [arXiv:0707.3650, hep-ph]; A. Falkowski, S. Pokorski, and M. Schmaltz, Twin SUSY, Phys. Rev. D74 (2006) 035003 [hep-ph/0604066]; S. Chang, L. J. Hall, and N. Weiner, A Supersymmetric twin Higgs, Phys. Rev. D75 (2007) 035009, [hep-ph/0604076].

[7] Z. Chacko, H.S. Goh, R. Harnik, The Twin Higgs: Natural electroweak breaking from mirror symmetry. Phys. Rev. Lett.96 (2006) 231802, hep-ph/0506256

[8] Z. Chacko, H.S. Goh, R. Harnik, A Twin Higgs model from left-right symmetry, JHEP 0601 (2006) 108, hep-ph/0512088

[9] T. Han, H.E. Logan, B. McElrath, L.T. Wang, Phenomenology of the little Higgs model, Phys. Rev. D 67 (2003) 095004

[10] H.S. Goh, S. Su, Phenomenology of The Left-Right Twin Higgs Model, Phys. Rev. D 75 (2007) 075010

[11] G. Brooijmans et al., New Physics at the LHC: A Les Houches Report. Physics at Tev Colliders 2007 – New Physics Working Group, arXiv:0802.3715 [hep-ph]

[12] L. P. E. Richter-Was, D. Froidevaux, ATLFAST 2.0, a fast simulation package for ATLAS, *ATLAS physics note.* ATL-PHYS-98-131 (1998).

[13] T. Sjostrand, S. Mrenna, and P. Skands, PYTHIA 6.4 physics and manual, *JHEP* **05** (2006) 026, `hep-ph/0603175`.

[14] S. Gonzalez de la Hoz, L. March, E. Ros, Search for hadronic decays of Z_H and W_H in the Little Higgs model, ATL-PHYS-PUB-2006-003

[15] the ATLAS collaboration, *ATLAS Computing System Commissioning note* **in preparation**.

[16] S. Frixione and B. Webber, Matching NLO QCD computations and parton shower simulations, *JHEP* 0206 (2002) 029, `hep-ph/0204244`.

[17] P. N. S. Frixione and B. Webber, Matching NLO QCD and parton showers in heavy flavour production, *JHEP* 0308 (2003) 007, `hep-ph/0305252`.